Photodetachment of Singly Solvated Halide Ions

Yarjing Yang,[†] Harrald V. Linnert,[‡] Jose M. Riveros,[‡] Kathryn R. Williams,[†] and John R. Eyler*,[†]

Department of Chemistry, University of Florida, P.O. Box 117200, Gainesville, Florida 32611-7200, and Instituto De Química, USP, Av. Lineu Prestes 748, Cid. Universitária, 05508−900 São Paulo, Brazil

Received: February 14, 1996; In Final Form: December 19, 1996[⊗]

Photodetachment in a Fourier transform ion cyclotron resonance (FT-ICR) mass spectrometer was used to measure the binding energies of $(CH_3OH)X^-$ (X = F, Cl, Br, I), $(ROH)Br^-$ (R = C_2H_5, *i*-C_3H_7, *n*-C_3H_7), and $(CH_3CN)Br^-$. The methanol complexes of F^- and Cl^- were prepared by sequential ion/molecule reactions, while equilibrium solvent exchange was used for preparation of the Br^- and I^- complexes. The photodetachment process was observed over the wavelength range of 260−350 nm using a tunable dye laser with a frequency-doubling accessory. Assuming that the photodetachment process leads to complete dissociation to the neutral solvent plus halogen atom, the binding energies were calculated by subtracting the known electron affinities of the halogens from the measured photodetachment thresholds. The binding energy values obtained for $(CH_3OH)F^-$, $(CH_3OH)Cl^-$, $(CH_3OH)Br^-$, $(CH_3OH)I^-$, $(C_2H_5OH)Br^-$, $(i\text{-}C_3H_7OH)Br^-$, $(n\text{-}C_3H_7OH)Br^-$, and $(CH_3CN)Br^-$ are 29.6, 18.7, 15.1, 14.4, 15.2, 16.5, 16.7, and 13.4 kcal/mol, respectively. On the basis of previously published theoretical potential surfaces for the neutral halogen−solvent system, the reported BEs may be high. For $(CH_3OH)F^-$ and $(CH_3OH)Cl^-$ the error should be only about 0.5 kcal/mol, but it may be 1−2 kcal/mol for the Br^- and I^- complexes. For the alcohol/halide adducts, the overall observation is an increase in binding energy with decreasing RO^- proton affinity and increasing X^- proton affinity.

Introduction

Fundamental studies of the thermodynamics of solvation are important for several reasons. First there is the chemistry of the solvation process itself. A free molecule or ion becomes surrounded by solvent molecules in the bulk medium. This results in changes in the interactions between solvent molecules, as well as the formation of new solute/solvent interactions, including hydrogen bonds in protic systems. Solvation is often the key factor in relative solubility effects, which are essential in many types of chemical separations. Also of practical significance is the role of solvation in chemical reactions. Since many reactions take place in solution, the solvent often has a pronounced effect on the reaction rate and position of equilibrium. Although the optimum solvent for a particular application may be identified by conducting a series of reactions, it would be more expedient to predict such effects from knowledge of the solvation of the reacting species. However, because of the accompanying changes in solvent structure and the solvation of counterions, it is often difficult to obtain meaningful data from measurements of the bulk materials. It is, therefore, desirable to study the thermodynamic aspects of solvation, in particular the binding energies of ion/solvent adducts, in the gas phase, where there is no interference from other species.

The binding of cations and anions to neutral molecules has been investigated by a variety of mass spectrometric techniques,[1−6] and solvated ions such as the water and alcohol-solvated halides have also been heavily studied.[7−23] These investigations have provided information about the stability of the hydrogen bond and the effects of structural variations in these compounds. Work involving ions surrounded by solvent clusters[9−14] has also led to a better understanding of the characteristic properties of bulk solutions.

Ion solvation energies have been measured by several methods. These have included equilibrium measurements in high-pressure[13−18] and ion cyclotron resonance[6−8] mass spectrometers (HPMS and ICR-MS), photodissociation[1−3] and photodetachment[9] in time-of-flight (TOF) instruments, and collisionally activated dissociation (CAD) in a guided-ion beam apparatus.[10] Photoelectron spectroscopy (PES)[5] and ICR-MS[4] have also been used for photodetachment experiments.

Although a large volume of thermodynamic data is available, there is still considerable disagreement in the literature about the binding energies (BEs) of solvated anions evaluated by different methods.[11−15,19−23] This may be attributed to the use of equilibrium methods, which can involve inherent uncertainties and may not give direct measurements of the binding energies. Kebarle and co-workers[13] have made extensive use of ion/solvent cluster reactions, represented by

$$XS_n^- \rightleftarrows XS_{n-1}^- + S, \quad \ln K_{n,n-1} = \Delta S/R - \Delta H/(RT) \qquad (1)$$

where X^- is the anion solvated by molecule S. The equilibrium is established in the ion source of a high-pressure mass spectrometer, and the equilibrium constant, $K_{n,n-1}$, is determined from intensity measurements of the two anions and the pressure of the solvent molecule, S. The enthalpy change can be determined by repeating the measurements at a series of temperatures.[11−13,20] Another equilibrium method[6−8,19,23] is a comparative procedure, utilizing data at a single temperature for a series of bimolecular exchange reactions of general form

$$S_1X^- + S_2 \rightleftarrows S_2X^- + S_1, \quad \Delta G = -RT \ln K \qquad (2)$$

This gives a relative value of the free energy of solvation within the series of investigated solvent molecules. The enthalpy change is then determined from the free energy after estimation of the entropy change.

[†] University of Florida.
[‡] Instituto De Química, USP.
[⊗] Abstract published in *Advance ACS Abstracts,* March 1, 1997.

S1089-5639(96)00451-3 CCC: $14.00

These equilibrium approaches are often prone to uncertainties. For example, Hiraoka and Yamabe[12] used both a gas-phase solvation reaction (eq 1) and an *ab initio* MO calculation with a 3-21G basis set to determine the BE of $(CH_3OH)F^-$ and obtained results of 23.3 ($\pm$1.0−2.0) and 26.2 kcal/mol, respectively. Using the bimolecular exchange method (eq 2), Larson and McMahon[19a] obtained 29.6 ($\pm$0.5−1.0) kcal/mol for the BE of the same anion. There is a difference of at least 6 kcal/mol in the two experimental results, and neither agrees with the *ab initio* calculation.

An alternative method for determining binding energies makes use of a photodetachment reaction. To a first approximation, the photodetachment process may be represented by

$$SX^- \xrightarrow{h\nu} S + X + e^- \qquad (3)$$

However, as described further under Results and Discussion, consideration of an intermediate loosely bound neutral complex may be necessary. The threshold for photodetachment is obtained by measuring the depletion of SX^- as a function of photon energy. This value can be used to calculate the BE of SX^-, if the electron affinity (EA) of X is known (from either established values or the photodetachment threshold of unsolvated X^-). Brauman *et al.*[24,25] have used this method to evaluate the EAs of several systems including organophosphines and aliphatic oxyl radicals. Similar measurements of photodissociation reactions (process similar to eq 3, but with the charge remaining on one of the products, presumably X) provide data on the BEs of solvated cations. For example, Brucat *et al.*[3] used photodissociation in a TOF mass spectrometer to obtain the upper limit of the ground-state adiabatic dissociation energy of $(H_2O)V^+$. The binding energies of $Mg(H_2O)_n^+$ ($n \geq 1$) were determined in Fuke's[1] and Duncan's[2] groups by the same technique. Johnson *et al.*[9] also used time-of-flight (TOF) mass analysis to demonstrate the competition between photodissociation and photodetachment in hydrated electron clusters, $(H_2O)_n^-$. They observed that photodetachment is the only process at high excitation energies. However as the photon energy decreases, photodissociation begins to compete with photodetachment.

Ion cyclotron resonance mass spectrometry is especially desirable for photodetachment studies, because ions may be trapped for extended periods and subjected to laser irradiation. Thus, it is feasible to form anion/solvent adducts by suitable ion/molecule reactions and to measure their BEs by the photodetachment process. This report presents results on several singly solvated halide ions. The solvent molecules include CH_3OH, C_2H_5OH, *i*-C_3H_7OH, *n*-C_3H_7OH, and CH_3CN. Riveros *et al.*[26−29] have developed methods for producing these adducts (as shown for specific cases in the next section) via ion/molecule reactions. These preparation procedures have been used successfully in our laboratory[30] to obtain IR spectra of solvent/halide adducts by IR multiphoton dissociation (IRMPD) measurements. In this work the binding energies of $(ROH)X^-$ and $(CH_3CN)Br^-$ have been determined by the photodetachment method using laser irradiation in the 260−350 nm wavelength range.

Experimental Procedures and Data Analysis

Instrumentation. The FT-ICR mass spectrometer used for this work was equipped with a 2 T superconducting magnet and a Bruker Aspect 3000 console with 512K memory (Figure 1). The vacuum chamber had 8 in. flanges on either end, one with three optical windows for transmission of laser radiation, the other with one window which allowed laser access to the filament side of the cell. This arrangement permitted easy alignment of the laser beam. The modified vacuum system, which was pumped by a 700 L/s diffusion pump, maintained the background pressure below 10^{-8} Torr. The partial pressures of the three reagents used for the preparation of the solvent/anion complexes were controlled by a pulsed valve and three precision leak valves on the inlet system.

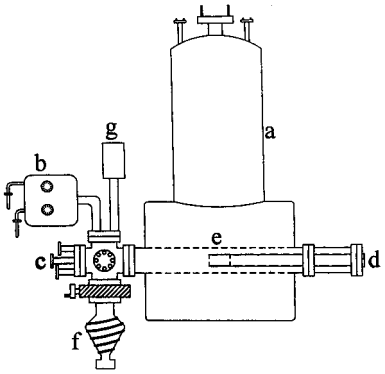

Figure 1. FT-ICR mass spectrometer: (a) 2 T superconducting magnet; (b) inlet system; (c) vacuum flange with three laser windows;(d) vacuum flange with one laser window and preamplifier connections to the electronics console; (e) cylindrical ICR cell; (f) diffusion pump; (g) ion gauge.

A cylindrical cell (6.0 cm diameter × 6.0 cm length) was used for the photodetachment experiments. The fine mesh at the front trapping plate was replaced with a coarse mesh to increase transmission of the laser beam and to allow the desired ions to be trapped without ionization of the metal by the laser beam. Because the volume of the cylindrical cell was much larger than that of conventional cubic cells used in this laboratory and elsewhere, space charge effects were reduced. The trapping potential was kept as low as possible (1.2−1.4 V) to prevent high-velocity ions from being trapped.

Radiation in the 260−350 nm range was provided by a tunable dye laser (Quantel TDL 50) with a frequency-doubling accessory. This was pumped by a Nd^{3+}:YAG laser (Quantel YG 581C), which was synchronized with the mass spectrometer using laboratory-built interface electronics.[31] The wavelength scan was controlled by commercial software provided with the dye laser. The wavelength accuracy of this laser system is $\pm$0.5 Å, and the resetting stability is $\pm$0.02 Å; the laser linewidth is 0.08 Å, and typical pulse lengths are 8 ns fwhm. Five different dyes (Fluorescein, Rhodamine 590, 610, and 640, and DCM) were needed to cover (after frequency doubling) the 260−350 nm range. The laser output power (*ca.* 8−15 mJ/pulse) was kept constant for each photodetachment spectrum.

Chemicals and Ion−Molecule Reactions. All chemicals were commercial products of spectral-grade purity and were used without further purification, except for several freeze−pump−thaw cycles. NF_3 was purchased from Air Products and Chemicals, Inc., phosgene was obtained from Matheson, optima-grade methanol was purchased from Fisher Scientific, and the rest of the samples were obtained from Aldrich.

The singly solvated halide ions were formed by the methods of Riveros.[26−29] A two-step procedure was used to produce the methanol adducts of fluoride and chloride.[26−28] In the first step the pertinent reagent gas (NF_3 for the F^- adduct; phosgene for the Cl^- adduct) underwent dissociative electron capture of 6−12 V electrons:

$$NF_3 + e^- \rightarrow NF_2 + F^- \qquad (4)$$

$$COCl_2 + e^- \rightarrow COCl^- + Cl \qquad (5)$$

The anions subsequently reacted with a second reagent gas to form the desired adduct:[29]

$$F^- + HCOOCH_3 \rightarrow (CH_3OH)F^- + CO \quad (6)$$

$$COCl^- + CH_3OH \rightarrow (CH_3OH)Cl^- + CO \quad (7)$$

The neutral carbon monoxide removed some excess energy resulting from these exoergic reactions, but a relaxation delay of 2.5−4 s was still required to allow the $(CH_3OH)F^-$ or $(CH_3OH)Cl^-$ to approach thermal equilibrium prior to the photodetachment measurements. For this work the thermalization time was determined by measuring the photodetachment threshold with increasing delay times (2−6 s), until no significant change was observed. Results of earlier IR dissociation experiments involving $(CH_3OH)F^-$ suggested that *ca.* 100 collisions between the ions and the bath gas (methyl formate) were required for thermalization.[32,33]

The preparation of $(CH_3OH)I^-$ and the adducts of Br^- with CH_3OH, C_2H_5OH, *i*-C_3H_7OH, *n*-C_3H_7OH, and CH_3CN required an alternate method involving the gas-phase exchange of $(H_2O)X^-$ with the desired solvent. Initially, hydroxide ions from dissociative electron capture by water reacted with bromo- or iodobenzene to produce the water adducts:

$$H_2O + e^- \rightarrow OH^- + H \quad (8)$$

$$OH^- + C_6H_5X \rightarrow (H_2O)X^- + C_6H_4 \quad (9)$$

Subsequently, $(H_2O)X^-$ was allowed to exchange with the solvent:

$$S + (H_2O)X^- \rightleftharpoons SX^- + H_2O \quad (10)$$

A period of 2 s was needed for the final reaction to reach equilibrium. Because the SX^- ions were already thermalized, no further relaxation delay was required.

For the electron capture reactions of NF_3, $COCl_2$, and H_2O, 12.0, 6.0, and 10.0 V electrons were used, respectively, and the gas pressures were $(4.0-5.0) \times 10^{-8}$ Torr. The total pressure was 8.0×10^{-8} Torr for the production of $(CH_3OH)F^-$ and $(CH_3OH)Cl^-$ and 1.5×10^{-7} Torr for the iodide and bromide adducts. The higher pressure in the latter experiments also helped to ensure that the I^- and Br^- adducts were properly thermalized.

Pulse Sequence. After a quench pulse, a 100−150 ms pulse of 6−12 V electrons was generated for dissociative capture by the first reagent gas (eqs 4, 5, and 8). This was followed by a 2.5−4 s delay for the ion/molecule reactions (eqs 6, 7, and 10), as well as thermal relaxation of the product solvated ions, as described above. After the delay, a series of single-frequency ejections was generated to remove undesired ions. The laser was then fired, followed by detection of the remaining solvent/anion adducts using a standard chirp excitation sweep. Data were acquired over a broad-band frequency range corresponding to $m/z = 15$ to $m/z = 1000$. One-hundred 32K point time-domain transients were signal-averaged for all ions except $(CH_3OH)F^-$ and $(CH_3OH)Cl^-$ (50 transients each). The absolute intensities of the solvent/anion adducts were recorded under the same conditions with and without blocking the laser beam.

Data Analysis. In a photodetachment experiment the ion signals, both before and after laser irradiation, are recorded as a function of the laser wavelength. Because the solvent/anion adduct is converted to neutral products, the ion concentration decreases if the laser pulse has sufficient energy to remove the electron. The number of ions remaining is related to the photodetachment cross section, $\sigma(\lambda)$, by[34]

$$N = N_0 e^{-k_p(\lambda)t} \quad (11)$$

in which t is the duration of the laser pulse and $k_p(\lambda)$ is the wavelength-dependent rate constant for the photodetachment process:

$$k_p(\lambda) = f \int \sigma(\lambda)\, \rho(\lambda)\, d\lambda \quad (12)$$

In eq 12, $\sigma(\lambda)$ is the cross section in cm^2, which is assumed to be constant over the narrow laser bandwidth, and $\rho(\lambda)$ is the photon flux in $cm^{-2}\ s^{-1}$. The unitless geometric factor, f, is the fraction of the photon beam's cross-sectional area that overlaps the collection of ions in the ICR cell. If absolute cross sections are needed, f may be evaluated from the beam diameter, the photon flux, and the sizes of the ion clouds. Although the ions are constrained to the center of the cell prior to ICR detection, in these experiments the spatial extension of the ion cloud is generally much larger than the laser beam diameter, and f is effectively unity.

Assuming $\sigma(\lambda)$ to be constant over the laser bandwidth, eq 11 may be substituted into eq 12, and suitable manipulations give[4]

$$\sigma(\lambda) = \ln(N_0/N)/ft \int \rho(\lambda)\, d\lambda \quad (13)$$

As stated above, the laser output power was kept constant throughout each photodetachment spectrum. Thus, the relative photodetachment cross section spectrum, which is sufficient for determination of the photodetachment threshold, may be obtained by plotting $\ln(N_0/N)$ versus the laser wavelength. At each wavelength setting the N and N_0 measurements were repeated four to six times, and the respective means and standard deviations were calculated. The standard deviations of the $\ln(N_0/N)$ values were subsequently propagated from the standard deviations of the data points and were used as error bars for the photodetachment spectra.

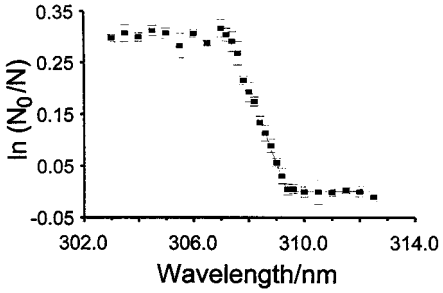

Figure 2. Photodetachment spectrum of $(C_2H_5OH)Br^-$: plot of $\ln(N_0/N)$ vs laser wavelength.

Figure 2 shows the $(C_2H_5OH)Br^-$ photodetachment spectrum, which is typical of all the spectra observed in this study. The $\ln(N_0/N)$ values rise steeply below the threshold wavelength (corresponding threshold energy evaluated precisely as described below), but there is significant curvature and flattening for laser wavelengths about 2−3 nm lower than the threshold. This may be attributed to the large photodetachment cross section, which totally depletes the ions within the volume irradiated by the laser beam, while ions in regions outside the beam path undergo no photodetachment.

For a given photodetachment spectrum, the initial fraction, κ, of the ICR ions contained in the volume irradiated by the laser should be constant:

$$\kappa = N_{0\ \mathrm{laser}}/N_{0\ \mathrm{ICR}} \tag{14}$$

(Note that κ, the fraction of ions irradiated by the laser beam, is not the same as f, the fraction of the laser beam that overlaps the ion cloud.) Because the ICR excitation sweep detects all the ions in the cell, the measured N_0 is equal to $N_{0\ \mathrm{ICR}}$, which can be separated into the ions in the irradiated volume, $N_{0\ \mathrm{laser}}$, and those not in the laser beam, $N_{0\ \mathrm{other}}$:

$$N_0{}^{\mathrm{ICR}} = N_{0\ \mathrm{laser}} + N_{0\ \mathrm{other}} = \kappa N_{0\ \mathrm{ICR}} + (1-\kappa)N_{0\ \mathrm{ICR}} \tag{15}$$

Because of the short duration of the laser pulse, there is insufficient time for the unirradiated population to diffuse into the laser region. Thus, the number of ions remaining in the irradiated region after the laser pulse is

$$N_{\mathrm{laser}} = N_{0\ \mathrm{laser}}\mathrm{e}^{-k_{\mathrm{p}}(\lambda)t} = \kappa N_{0\ \mathrm{ICR}}\mathrm{e}^{-C\sigma(\lambda)} \tag{16}$$

in which C represents the constant term $ft\int\rho(\lambda)\,\mathrm{d}\lambda$. Because the $N_{0\ \mathrm{other}}$ are still present, the total number of ions detected in the ICR cell following laser irradiation is given by

$$N_{\mathrm{ICR}} = N_{\mathrm{laser}} + N_{0\ \mathrm{other}} = \kappa N_{0\ \mathrm{ICR}}\mathrm{e}^{-C\sigma(\lambda)} + (1-\kappa)N_{0\ \mathrm{ICR}} \tag{17}$$

Rearrangement of eq 17 gives

$$\mathrm{e}^{C\sigma(\lambda)} = \frac{\kappa}{(\kappa-1) + (N/N_0)_{\mathrm{ICR}}} \tag{18}$$

in which $(N/N_0)_{\mathrm{ICR}}$ is the ratio of ions actually detected by the instrument following and before laser irradiation. The resulting equation for the photodetachment cross section is

$$\sigma(\lambda) = \frac{1}{C}\ln\left[\frac{\kappa}{(\kappa-1) + (N/N_0)_{\mathrm{ICR}}}\right] \tag{19}$$

Referring to Figure 2, the value of $\ln(N_0/N)$ becomes constant when N_{laser} is zero (*i.e.*, when the photodetachment process for ions in the laser beam is saturated). According to eq 17, this means that $(N/N_0)_{\mathrm{ICR}}$ equals $(1-\kappa)$. To evaluate κ, the $\ln(N_0/N)$ values were first plotted as shown in Figure 2 to locate the scattered points in the flattened part. The average of the corresponding N/N_0 ratios was set equal to $(1-\kappa)$, and the resulting value of κ was used to calculate the logarithmic function in eq 19 for the remaining points.

At the threshold, the cross section for optical detachment of an electron depends only on the long-range interaction between the two product particles. For polyatomic anions[36] with C_s symmetry, the cross section, which in this case can be expressed as $\sigma(E)$ rather than $\sigma(\lambda)$, is directly proportional to the square root of the energy in excess of the threshold, $(E-E_{\mathrm{T}})^{1/2}$:

$$\sigma(E) \propto (E-E_{\mathrm{T}})^{1/2} \tag{20}$$

or

$$\ln(F) = \alpha(E-E_{\mathrm{T}})^{1/2} \tag{21}$$

in which F is given by the expression in square brackets in eq 19 and α is a constant. To determine the threshold energy, an approximate E_{T} value was chosen from the plot of $\ln(F)$ versus λ, and experimental data points (E, $\ln F$) were substituted into eq 21 to obtain a series of initial α values. The mean ($\bar{\alpha}$) and standard deviation of the points about the mean were calculated. This procedure was repeated for decreasing E_{T}'s (at intervals of 0.01 kcal/mol), until the $\bar{\alpha}$ giving the minimum standard deviation was obtained. Throughout the analysis, plots of $\ln(F)$ versus $\bar{\alpha}(E-E_{\mathrm{T}})^{1/2}$ (Figure 3) were inspected visually to ensure that the calculated lines were, in fact, giving successively better fits to the data points in the threshold region.

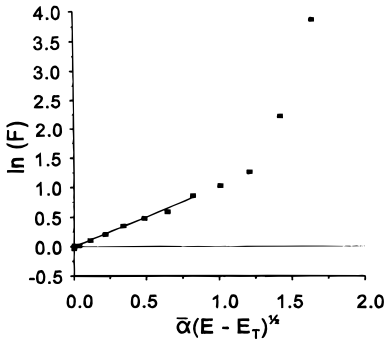

Figure 3. Plot of $\ln\{\kappa/[(\kappa-1) + (N/N_0)_{\mathrm{ICR}}]\}$ vs $\bar{\alpha}(E-E_{\mathrm{T}})^{1/2}$ for $(C_2H_5OH)Br^-$ with $\kappa = 0.30$ and best-fit value of $\bar{\alpha} = 3.1$.

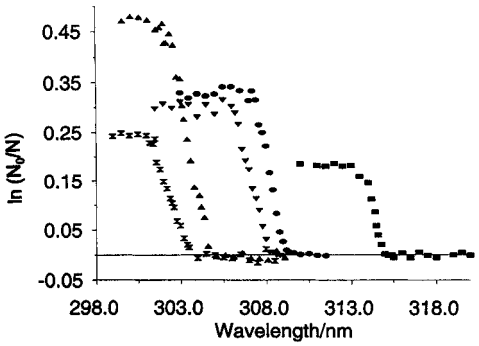

Figure 4. Photodetachment spectra: (■) $(CH_3CN)Br^-$; (●) $(CH_3OH)Br^-$; (▼) $(C_2H_5OH)Br^-$; (▲) $(i\text{-}C_3H_7OH)Br^-$; (⧗) $(n\text{-}C_3H_7OH)Br^-$.

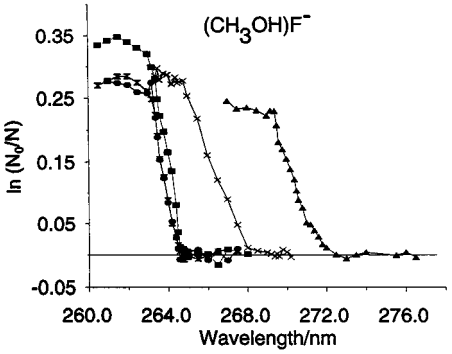

Figure 5. Photodetachment spectra of $(CH_3OH)F^-$ obtained using different thermalization times (t): (▲) $t = 2.34$ s; (×) $t = 3.20$ s; (■) $t = 3.77$ s; (⧗) $t = 4.31$ s; (●) $t = 6.05$ s.

Results and Discussion

The relative photodetachment spectra for bromide ion singly solvated with CH_3OH, C_2H_5OH, $i\text{-}C_3H_7OH$, $n\text{-}C_3H_7OH$, and CH_3CN are presented in Figure 4. As explained above, a delay period was required to ensure that the gas-phase exchange reactions for the preparation of the Br^- and I^- adducts (eq 10) reached equilibrium and that $(CH_3OH)F^-$ and $(CH_3OH)Cl^-$ (eqs 6 and 7) were properly thermalized. Figures 5 and 6 show photodetachment spectra for $(CH_3OH)F^-$ and $(CH_3OH)Cl^-$, respectively, obtained with increasing delay times. Studies of the bromide systems showed results similar to $(CH_3OH)Cl^-$. The reaction of fluoride ion with methyl formate (eq 6) is very exothermic, and a delay of about 4 s was required for collisional and radiative cooling of the $(CH_3OH)F^-$ ions. Because the newly formed $(CH_3OH)Cl^-$ ions were less energetic, they

TABLE 1: Electron Affinities[39a] (EA), Proton Affinities[39b] (PA), and Bond Dissociation Energies[39c] (*D*) of Species Studied in This Work

halogen	EA/kcal mol^{-1} ( ) = /kJ mol^{-1}	anion	PA/kcal mol^{-1} ( ) = /kJ mol^{-1}	bond	*D*/kcal mol^{-1} ( )/kJ mol^{-1}
F	78.37 (327.8)	OH^-	390.8 (1635)	H−OCH_3	104.4 (436.8)
Cl	83.44 (349.0)	CH_3O^-	381.4 (1595)	H−F	136.2 (569.9)
Br	77.45 (323.9)	$C_2H_5O^-$	377.8 (1580)	H−Cl	103.2 (431.6)
I	70.53 (295.0)	*i*-$C_3H_7O^-$	376.0 (1573)	H−Br	87.6 (366.4)
		n-$C_3H_7O^-$	376.4 (1574)	H−I	71.3 (298.4)
		t-$C_3H_7O^-$	374.9 (1564)	H−CH_2CN	93.0 (389)
		CH_2CN^-	372.2 (1557)		
		F^-	371.3 (1553)		
		Cl^-	333.3 (1394)		
		Br^-	323.6 (1353)		
		I^-	314.3 (1315)		

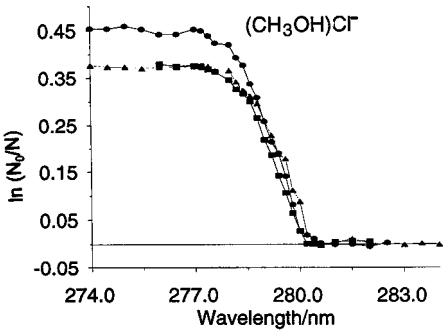

Figure 6. Photodetachment spectra of $(CH_3OH)Cl^-$ obtained using different thermalization times (*t*): (●) $t = 2.05$ s; (▲) $t = 3.20$ s; (■) $t = 4.34$ s.

reached thermal equilibrium in about 2.5 s. The 2.5 s delay was also sufficient for the exchange reactions (eq 10) to reach equilibrium.

By a thermochemical cycle for the photodetachment process (eq 3) the threshold is equal to the sum of the binding energy of the solvent/anion complex and the electron affinity of the halogen, with a small correction as described below. Thus, the BEs may be calculated from the thresholds and the known EAs given in Table 1. Table 2 presents the thresholds and binding energies for all complexes studied in this work. Results of previous investigations are also included.

This interpretation of the photodetachment threshold assumes that the vertical transition proceeds to a repulsive state which dissociates to form the solvent plus the free halogen, and not to a neutral bound complex. If there is excitation to a bound state, the photodetachment reaction would be

$$SX^- \xrightarrow{h\nu} SX + e^- \qquad (22)$$

instead of eq 3. For these solvent/anion complexes, it is expected that dissociation to S plus X (eq 3) occurs, as supported by several arguments. On the basis of experimental and calculated results of Brauman's group,[4,38] the preferred reaction is expected to depend on the Franck−Condon overlap of the ground-state vibrational wave function of the anion/solvent adduct with that of the neutral complex having the same geometry. In the ground-state anion/alcohol complexes, the position of H between the O and X nuclei may be predicted from the relative proton affinities (PAs) of RO^- and X^-, which are listed in Table 1. In all cases, X^- has a lower PA than RO^-, indicating that the H is closer to the oxygen (RO^-−$H^+\cdots X^-$). A vertical transition produces a neutral with the same internuclear distance, which should dissociate to form ROH + X.

The reaction of fluorine with methanol was studied theoretically by Glauser and Koszykowski,[40] who performed *ab initio* calculations using the MP2/6-31G(d,p) basis set. For hydroxyl-group attack, the results showed a nearly flat potential surface connecting the reactants and products, although there is a small energy minimum (BE = 3.2 kcal/mol) corresponding to a hydrogen-bonded complex (CH_3O−H···F) on the reactant surface. Brauman *et al.*[4,38] also carried out theoretical studies to interpret their photodetachment results for $(ROH)X^-$ (R = CH_3, $C_6H_5CH_2$, X = F, OCH_3). As predicted by the proton-affinity argument, Brauman's *ab initio* calculations indicate that the structure of the solvated anion is essentially RO−H···F^- with vertical detachment to a neutral complex resembling ROH plus F. The theoretical results of these two groups were used with the proton affinities and bond dissociation energies in Table 1 to construct representative potential energy surfaces for the methanol/halide systems. As shown in Figure 7, the anion/solvent adducts undergo photodetachment to the rising surface of the transition state for neutral hydrogen abstraction. The initially photodetached species subsequently reverts to the dissociated neutrals, ROH + halogen.

Presuming this model to be correct, Figure 7 shows that the BE calculated from the photodetachment threshold is higher than the true BE by the amount ΔE. The magnitude of this error may be estimated from the results of Glauser and Koszykowski[40] for the hydrogen abstraction reaction of methanol by fluorine. Their calculations indicate that the barrier height is 1.89 kcal/mol for methyl-group attack and negligible for hydroxyl-group attack. Using these results, the upper limit for the absolute error of the $(CH_3OH)F^-$ binding energy calculated from the photodetachment threshold should be no greater than 0.5 kcal/mol. Thus, the measured BE for $(CH_3OH)F^-$ is within experimental error of the values obtained by McMahon's group[19,22] (Table 2), although the experimental and calculated results of Hiraoka and Yamabe are several kcal/mol lower.

Bradforth *et al.*[41] studied the hydrogen abstraction reactions of fluorine with methanol and ethanol (F + HOR → HF + OR) via photodetachment of $(ROH)F^-$ (R = CH_3, C_2H_5). They observed photoelectrons corresponding to photodetachment to the product side of the upper surface in Figure 7a. Their data indicate that a threshold to produce CH_3O + HF should occur at 385 nm. However, this spectral region was not examined in the present studies, because, as shown in Figure 5, there was no evidence of any anion loss at wavelengths above about 264 nm for the cooled $(CH_3OH)F^-$. We can give no further explanation for the apparent absence of photodetachment at wavelengths longer than 264 nm in our studies, other than perhaps a lower photodetachment detection sensitivity in this work compared to that of Bradforth *et al.*

As Table 2 shows, the BEs for the other methanol/halide adducts obtained using this approach are about 1−3 kcal/mol higher than literature values. This may be due to greater ΔE's for these systems, but preliminary calculations[42] indicate that

TABLE 2: Photodetachment Threshold (E_T) and Binding Energies (BE) of Singly Solvated Halides

	this work		other experimental results		calculated results	
	E_T/kcal mol^{-1} ( ) = nm	BE/kcal mol^{-1} ( ) = /kJ mol^{-1}	BE/kcal mol^{-1} ( ) = /kJ mol^{-1}	method[a] [ref]	BE/kcal mol^{-1} ( ) = /kJ mol^{-1}	method or basis set [ref]
$(CH_3OH)F^-$	108.0	29.6 ± 0.5	29.6 (123.8)	EX [19]	26.2 (109.6)	3-21 G [12]
	(265.7)	(123.8 ± 2.1)	30.6 (128.0)	EQ [22]		
			23.3 (97.5)	EQ [12]		
$(CH_3OH)Cl^-$	102.1	18.7 ± 0.5	16.8 (70.2)	EX [19]	16.2 (67.8)	3-21 G [12]
	(280.9)	(78.2 ± 2.1)	16.3 (68.2)	EQ [15]		
			14.2 (59.4)	EQ [13,14]		
			17.4 (72.8)	EQ [12,20]		
$(CH_3OH)Br^-$	92.5	15.1 ± 0.4	13.9 (58.1)	EQ [12]	16.0 (66.9)	3-21 G [12]
	(309.5)	(63.2 ± 1.7)			12.9 (54.0)	MP4/SDTQ [23]
$(CH_3OH)I^-$	84.9	14.4 ± 0.4	11.3 (47.3)	EQ [13,14]	10.8 (45.2)	3-21 G [12]
	(337.3)	(60.2 ± 1.7)	11.2 (46.8)	EQ [12]		
$(C_2H_5OH)Br^-$	92.7	15.2 ± 0.6	14.4 (60.2)	EX [23]		
	(309.3)	(63.6 ± 2.5)				
$(i\text{-}C_3H_7OH)Br^-$	93.9	16.5 ± 1.2	14.6 (61.1)	EX [23]		
	(304.8)	(69.0 ± 5.0)				
$(n\text{-}C_3H_7OH)Br^-$	94.1	16.7 ± 0.4				
	(304.2)	(70.0 ± 1.7)				
$(CH_3CN)Br^-$	90.9	13.4 ± 0.9	12.7 (53.1)	EX [23]	11.0 (45.9)	MP4 [23]
	(315.3)	(56.1 ± 3.8)	12.9 (54.0)	EQ [20b]		
$(CH_3CN)Cl^-$			15.8 (66.1)	EX [19]		
			14.0 (58.6)	EQ [15]		
			13.4 (56.0)	EQ [13,14]		
$(CH_3CN)F^-$					16.0 (66.9)	3-21G [11]

[a] EQ = gas-phase equilibrium. EX = bimolecular exchange.

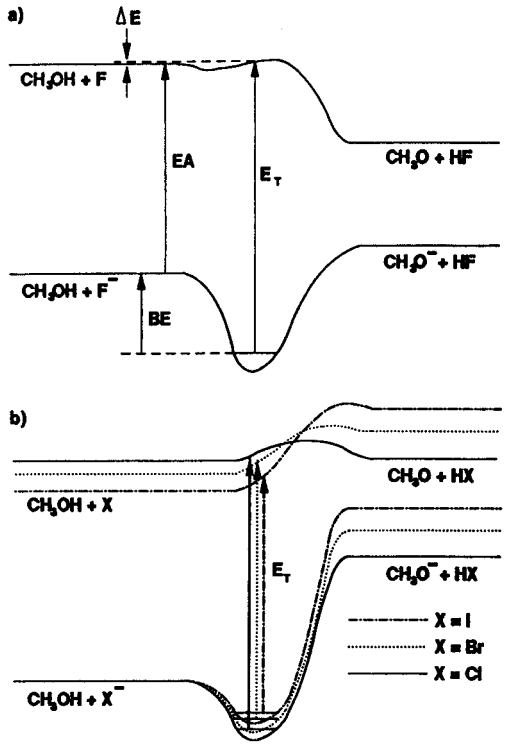

Figure 7. Model potential energy curves for methanol/halide ion adducts and corresponding neutral species: (a) $(CH_3OH)F^-$; (b) $(CH_3OH)Cl^-$, $(CH_3OH)Br^-$, and $(CH_3OH)I^-$. Lower curves represent the interaction of the CH_3OH and halide from infinite separation to a stable bound state. Vertical distances between reactant and product asymptotes are consistent with reaction energies calculated from the proton affinities in Table 1, and depths of the potential wells are consistent with the BEs obtained in this work. Upper curves represent neutral hydrogen abstraction reactions, with vertical distances consistent with reaction energies calculated from the bond dissociation energies in Table 1. In a, the upper curve is also consistent with the theoretical results of ref 41. Upper curves in b are reasonable models, based on the endothermicity of the hydrogen abstraction reactions.

the magnitude is very small for the alcohol/chloride adducts. Because of the greater polarizabilities of the heavier halogens (Br and I), spin−orbit coupling with the alcohol is expected in the Br and I complexes. This would lead to a more gradually rising potential energy surface and a greater value of ΔE for complexes with these atoms. Measurement of the kinetic energies of the separating neutrals (ROH and X) at threshold, or extrapolations from kinetic energies of photodetached electrons above threshold, would allow ΔE to be evaluated directly. Lacking such data, an estimate of the minimum height for the methanol complexes may be obtained from thermochemical data (Table 1) for neutral hydrogen abstraction reactions (overall reaction depicted by the upper curves in Figure 7):

$$Cl + CH_3OH \rightarrow HCl + CH_3O \qquad \Delta H = 1.2 \text{ kcal/mol} \tag{23}$$

$$Br + CH_3OH \rightarrow HBr + CH_3O \qquad \Delta H = 16.8 \text{ kcal/mol} \tag{24}$$

$$I + CH_3OH \rightarrow HI + CH_3O \qquad \Delta H = 33.1 \text{ kcal/mol} \tag{25}$$

The reaction barrier must be at least as high as the endothermicity of these reactions. It is probable that the trend of the barrier heights may be similar to the ΔH trend, *i.e.*, much larger for Br and I than for F or Cl. For very endothermic reactions, it is generally true that the structure of the transition state reached via photodetachment is similar to that of the products. However, the relative bond lengths (discussed below) indicate that the neutral complex is very similar to the reactants. Thus, the complex must be located very low on the rising surface, and the corresponding ΔE must be much less than the overall barrier height. Given this argument, the ΔEs for Br and I complexes should be greater than those for F and Cl complexes, but only by 1−2 kcal/mol. As explained in the Introduction, there is some uncertainty in the BE values obtained by equilibrium methods, although error bars are not given by the cited authors. Examination of their data indicates a random uncertainty of about ±1−2 kcal/mol in the reported BEs. Furthermore, binding energies determined by equilibrium methods are subject to systematic error in the statistical

mechanical estimation of ΔS, which is based on the vibrational frequency of the H−X bond in ROH−X$^-$. As the halide becomes heavier, the vibrational frequency of the ROH−X$^-$ bond decreases. It is possible that the vibrational frequency has not been estimated correctly by previous authors. This would produce a systematic error in the entropy change, which would subsequently affect the reported BE.

Results of *ab initio* calculations support the relative bond-length predictions and also provide informative bond-angle data. Del Bene[43] studied the water adducts of F$^-$ and Cl$^-$, (HOH)F$^-$ and (HOH)Cl$^-$, using the Hartree−Fock 6-31G(d) and MP2/6-31+G(2d,2p) basis sets for the optimized structures and stabilization energies, respectively. The fluoride complex exhibits a conventional hydrogen-bonded structure with an essentially linear O−H−F system, and internuclear distances of 1.038 Å and 1.379 Å for the O−H and H−F bonds, respectively. Consistent with the lower proton affinity of Cl$^-$, the bond lengths in (HOH)Cl$^-$ are 0.961 Å (O−H) and 2.305 Å (H−Cl). However, the bond is bent, with an O−H−Cl angle of 18.6°. The same trends were observed by Hiroaka and Yamabe[12] in their calculations on (CH$_3$OH)X$^-$ complexes. In all cases the H−X bond is longer than the O−H bond. The H−X bond length increases in the order F < Cl < Br < I, while the calculated BEs show the reverse order. In agreement with Del Bene's work, the hydrogen bond is linear in (CH$_3$OH)F$^-$ and nonlinear in the other methanol/halide adducts. The higher level *ab initio* calculations of (CH$_3$OH)F$^-$ of Wladkowski *et al.* indicate a slight deviation from linearity (O−H−F bond angle of 175.5°). Results obtained by Hiraoka and Mizuse[20a] on Cl$^-$(ROH)$_n$ (R = OH, CH$_3$, C$_2$H$_5$, *n*-C$_3$H$_7$, *i*-C$_3$H$_7$, *t*-C$_4$H$_9$) using the *ab initio* 3-21G and 4-31G+p (0.07) basis sets also show that the RO−H−Cl bond is bent in these complexes. For the 3- and 4-carbon alcohols, this allows the Cl$^-$ to interact with both the hydroxyl and methyl hydrogens to form a "chelate" structure.

Considering the adduct of CH$_3$CN with Br$^-$, it is presumed that a situation similar to that depicted in Figure 7b is favored by a loose interaction of the bromide ion with CH$_3$CN. Yamabe and Hiraoka optimized the geometry for (CH$_3$CN)F$^-$ and (CH$_3$CN)Cl$^-$ using the 4-31G+p GTO basis set.[11] The charge distribution indicates that CH$_3$CN is described by H$_3^{\delta+}$−C$^{\delta-}$−C$^{\delta+}$≡N, rather than CH$_3$C$^{\delta+}$≡N$^{\delta-}$, with the methyl hydrogens having more positive character than the center carbon. According to their calculations, the most stable structure for (CH$_3$CN)F$^-$ has C_s symmetry with the F$^-$ bound to one of the three hydrogens in the methyl group via a linear F−H−C bond and F−H and H−C bond distances of 1.70 and 1.14 Å, respectively. The bond lengths in (CH$_3$CN)Cl$^-$ are 2.70−3.00 and 1.09 Å for the Cl−H and H−C bonds, respectively. Recently, similar results were obtained by Riveros *et al.*,[23] who optimized the geometries for solvated anions at the MP4(SDTQ) level. In (CH$_3$CN)Br$^-$ the Br$^-$ is bonded collectively to the methyl hydrogens, with Br−H and H−C bond distances of 3.27 and 1.1 Å, respectively. Thus, all the calculated results for (CH$_3$CN)X$^-$ complexes indicate a loose interaction of X$^-$ with the solvent, which should lead to the photodetachment process shown in Figure 7. The endothermicity of the hydrogen abstraction reaction of Br with CH$_3$CN,

$$\mathrm{Br} + \mathrm{CH_3CN} \rightarrow \mathrm{HBr} + \mathrm{CH_2CN} \qquad \Delta H = 5.4 \text{ kcal/mol} \tag{26}$$

is much less than that for Br + CH$_3$OH (eq 17). Considering the very loose interaction in the neutral (CH$_3$CN)Br complex, the ΔE is expected to be very small for this system. This is supported by the close agreement of the BE with previous results.

Although the threshold data in Table 2 were obtained at room temperature, these results should also be valid at 0 K. As argued above, the photodetachment process initially produces a neutral of the same geometry as the adduct ion. Subsequently, the neutral dissociates to the solvent molecule and halogen atom. In this process, there is a net conversion of three vibrational modes to the three translational degrees of freedom of the halogen atom. Of particular importance in the alcohol adducts is the ROH−X stretch, which roughly corresponds to the reaction coordinate on the upper surfaces in Figure 7. Excitation of this mode in the solvated anion may, at first thought, lead to a reduction in the threshold energy. To examine this possibility, the vibrational data for (CH$_3$OH)F$^-$ and CH$_3$OH obtained from the theoretical studies of Wladkowski *et al.*[38] were used to calculate the error in the threshold value. In (CH$_3$OH)F$^-$, the only three vibrations that are active at room temperature occur at 75 (ν_{15}), 177 (ν_{10}), and 420 (ν_9) cm^{-1}, to give a contribution of 1.1 kcal/mol. In CH$_3$OH the vibrationally active modes are ν_{12} and ν_8 at 269 and 1036 cm^{-1}, respectively. The corresponding energy contribution is 0.3 kcal/mol, which, when added to 0.9 kcal/mol for the three new translational degrees of freedom, is essentially equal to the room-temperature vibrational energy of (CH$_3$OH)F$^-$ (given the uncertainties of the calculated vibrational frequencies). Considering that the nascent product may not be at thermal equilibrium, there may be a small positive error in the threshold due to this effect. However, the 420 cm^{-1} mode (ROH−X stretch) can be calculated ($h\nu/[e^{h\nu/kt} - 1]$) to contribute only 0.18 kcal/mol to the energy of the anion. Even if the nascent product were to retain all of this energy, the error produced would be small compared to the 0.5−2 kcal/mol estimate for ΔE, as discussed previously. It is a reasonably safe assumption that the same trend holds for the other complexes studied. Thus, the reported thresholds should be the same at either 298 or 0 K. Since the halide electron affinities used in the data analysis are zero-kelvin values,[39a] the binding energies in Table 2 are valid at 0 K, with the proviso that the ΔE is small, as described above. Because the usual ΔnRT correction is zero at 0 K, the BE values also represent enthalpy changes at 0 K.

Conclusions

The results in Table 2 show that the binding energy trend is I$^-$ < Br$^-$ < Cl$^-$ ≪ F$^-$ for the methanol adducts. The BE difference for (CH$_3$OH)F$^-$ compared to (CH$_3$OH)Cl$^-$ is 10.9 kcal/mol, whereas the (CH$_3$OH)Cl$^-$/(CH$_3$OH)Br$^-$ and (CH$_3$OH)-Br$^-$/(CH$_3$OH)I$^-$ differences are only 3.6 and 0.7 kcal/mol, respectively. The same order and approximate differences were found by previous investigators. Thus, these data generally confirm the results of previous measurements, which utilized entirely different experimental approaches. Referring to Table 1, this is also the trend of the proton affinities of the halide ions. For the complexes with bromide ion, the BE order is CH$_3$-OH < C$_2$H$_5$OH < *i*-C$_3$H$_7$OH < *n*-C$_3$H$_7$OH, which is the same as the order of the alkyl-group size, but opposite the RO$^-$ proton-affinity order. Thus, for the alcohol/halide adducts, the overall observation is an increase in BE with decreasing RO$^-$ proton affinity and increasing X$^-$ proton affinity. As the hydrogen becomes more loosely bound to the alcohol oxygen, it is more available for bonding to X$^-$.

The results of this and previous work on solvated bromide anions, as well as other studies of chloride complexes, show that complexes of these halides with acetonitrile have BEs about

1−2 kcal/mol lower than the methanol adducts. However, calculated results show that the BE for $(CH_3CN)F^-$ is more than 7 kcal/mol less than that for $(CH_3OH)F^-$. The difference in behavior of F^- compared to Cl^-, Br^-, and I^- can be understood in terms of the calculated geometries discussed above. The $(CH_3OH)Cl^-$, $(CH_3OH)Br^-$, and $(CH_3OH)I^-$ complexes have nonlinear CH_3O-H-X hydrogen bonds, and the results indicate that there is additional interaction of X^- with the methyl hydrogens. However, because of its small size, the F^- cannot interact with the methyl group in CH_3O-H-F^-, resulting in a nearly linear hydrogen bond. As stated above, the halide ion bonds via the methyl hydrogens in all the $(CH_3CN)X^-$ complexes. Thus, the bonding is somewhat similar for the CH_3OH and CH_3CN adducts of Cl^- and Br^-, and this is reflected in the closeness of the BEs of the $(CH_3OH)X^-$ and $(CH_3CN)X^-$ complexes for these halides. The bonding situation in $(CH_3OH)F^-$ is different from that in $(CH_3CN)F^-$, leading to a considerably greater BE for the methanol adduct.

Acknowledgment. The financial support of the U.S. Office of Naval Research, National Science Foundation (CHE 9311614 and U.S.-Brazil Cooperative Science Program), and the CNPq (Brazilian Research Council) is gratefully acknowledged. The authors would like to thank Dr. Philip Brucat for helpful suggestions and comments and Mr. Eric Milgram for preparing Figure 1.

References and Notes

(1) Misaizu, F.; Sanekata, M.; Tsukamoto, K.; Fuke, K.; Iwata, S. *J. Phys. Chem.* **1992**, *96*, 8259.

(2) Yeh, C. S.; Willey, K. F.; Robbins, D. L.; Pilgrim, J. S.; Duncan, M. A. *Chem. Phys. Lett.* **1992**, *196*, 233.

(3) Lessen, D. E.; Asher, R. L.; Brucat, P. J. *J. Chem. Phys.* **1990**, *93*, 6102.

(4) Moylan, C. R.; Dodd, J. A.; Han, C.; Brauman, J. I. *J. Chem. Phys.* **1987**, *86*, 5350.

(5) Bradforth, S. E.; Arnold, D. W.; Metz, R. B.; Weaver, A.; Neumark, D. E. *J. Phys. Chem.* **1991**, *95*, 8066.

(6) (a) Larson, J. W.; McMahon, T. B. *J. Am. Chem. Soc.* **1985**, *107*, 2612; (b) Larson, J. W.; McMahon, T. B. *J. Am. Chem. Soc.* **1985**, *107*, 766.

(7) Larson, J. W.; McMahon, T. B. *J. Am. Chem. Soc.* **1988**, *110*, 7604.

(8) Caldwell, G.; Rozeboom, M. D.; Kiplinger J. P.; Bartmess, J. E. *J. Am. Chem. Soc.* **1984**, *106*, 4660.

(9) Posey, L. A.; Campagnola, P. J.; Johnson, M. A. *J. Chem. Phys.* **1989**, *91*, 6536.

(10) Dalleska, N. F.; Honma, K.; Sunderlin, L. S.; Armentrout, P. B. *J. Am. Chem. Soc.* **1994**, *116*, 3519.

(11) Yamabe, S.; Hiraoka K. *Chem. Phys. Lett.* **1981**, *84*, 598.

(12) Hiraoka, K.; Yamabe, S. *Int. J. Mass Spectrom. Ion Proc*esses **1991**, *109*, 133.

(13) (a) Yamdagni, R.; Payzant, J. D.; Kebarle, P. *Can. J. Chem.* **1973**, *51*, 2507. (b) Arshadi, M.; Yamdagni, R.; Kebarle, P. *J. Phys. Chem.* **1970**, *74*, 1475. (c) Yamdagni, R.; Kebarle, P. *J. Am. Chem. Soc.* **1972**, *94*, 2940.

(14) (a) Caldwell, G.; Kebarle, P. *J. Am. Chem. Soc.* **1984**, *106*, 967; (b) *J. Am. Chem. Soc.* **1985**, *107*, 2612.

(15) (a) Meot-Ner (Mautner), M. *J. Am. Chem. Soc.* **1988**, *110*, 3858; (b) *J. Am. Chem. Soc.* **1988**, *110*, 3854.

(16) Sharma, R. B.; Blades, A. T.; Kebarle, P. *J. Am. Chem. Soc.* **1984**, *106*, 510.

(17) Meot-Ner (Mautner), M. *J. Am. Chem. Soc.* **1988**, *110*, 7604.

(18) (a) Meot-Ner (Mautner), M. *J. Am. Chem. Soc.* **1986**, *108*, 7525; (b) *J. Am. Chem. Soc.* **1988**, *110*, 3071.

(19) (a) Larson, J. W.; McMahon, T. B. *J. Am. Chem. Soc.* **1983**, *105*, 2944. (b) Larson, J. W.; McMahon, T. B. *J. Am. Chem. Soc.* **1984**, *106*, 517. (c) Larson, J. W.; McMahon, T. B. *Can. J. Chem.* **1984**, *62*, 675.

(20) (a) Hiraoka, K.; Mizuse, S. *Chem. Phys.* **1987**, *118*, 457. (b) Hiraoka, K.; Mizuse, S.; Yamabe, S. *J. Phys. Chem.* **1988**, *92*, 3934.

(21) Schuster, P. *Electron-Solvent and Anion-Solvent Interactions*, Kevan, L., Webster, B. C., Eds.; Elsevier Science: New York, 1976; Chapter 8.

(22) Szulejko, J. E.; Wilkinson, F. E.; McMahon, T. B. *Proceedings of the 37th ASMS Conference on Mass Spectrometry and Allied Topics*, May 21−26, 1989, Miami Beach, FL; p 333.

(23) Tanabe, F. K. J.; Morgon, N. H.; Riveros, J. M. *J. Phys. Chem.* **1996**, *100*, 2862.

(24) Janousek, B. K.; Zimmerman, A. H.; Reed, K. J.; Brauman, J. I. *J. Am. Chem. Soc.* **1978**, *100*, 6142.

(25) Berger, S.; Brauman, J. I. *J. Am. Chem. Soc.* **1992**, *114*, 4737.

(26) (a) Blair, L. K.; Isolani, P. C.; Riveros, J. M. *J. Am. Chem. Soc.* **1973**, *95*, 1057. (b) Isolani, P. C.; Riveros, J. M. *Chem. Phys. Lett.* **1975**, *33*, 362.

(27) Riveros, J. M.; Breda, A. C.; Blair, L. K. *J. Am. Chem. Soc*. **1973**, *95*, 4066.

(28) Faigle, J. F. G.; Isolani, P. C.; Riveros, J. M. *J. Am. Chem. Soc*. **1976**, *98*, 2049.

(29) Riveros, J. M.; Ingemann, S.; Nibbering, N. M. M. *J. Am. Chem. Soc.* **1991**, *113*, 1053.

(30) Peiris, D; Riveros, J. M.; Eyler, J. R. *Int. J. Mass Spectrom. Ion Processes* **1996**, *159*, 169.

(31) Moini, M.; Eyler, J. R. *J. Chem. Phys.* **1988**, *88*, 5512. The KIM microcomputer described in this reference has now been replaced by a (slightly) upgraded computer system, which is an Apple II computer with a John Bell Co. interface card.

(32) Wetzel, D. M.; Brauman, J. I. *Chem. Rev.* **1987**, *87*, 607.

(33) Rosenfeld, R. N.; Jasinski, J. M.; Brauman, J. I. *J. Am. Chem. Soc.* **1979**, *101*, 3999.

(34) (a) Branscomb, L. M. *Atomic and Molecular Processes*; Bates, D. R., Ed.; Academic: New York, 1962; p 112. (b) Smith, S. J. *Methods Exp. Phys.* **1972**, *7a*, 179.

(35) Steiner, B. J. *J. Chem. Phys.* **1968**, *49*, 5097.

(36) Brauman, J. I. *Gas Phase Ion Chemistry: Ions and Light*; Bowers, M. T., Ed.; Academic: New York, 1984; Vol. 3, Chapter 21.

(37) Bevington, P. R. *Data Reduction and Error Analysis for the Physical Sciences*; McGraw-Hill: New York, 1969; Chapter 6.

(38) Wladkowski, B. D.; East, A. L. L.; Mihalick, J. E.; Allen, W. D.; Brauman, J. I. *J. Chem. Phys.* **1994**, *100*, 2058.

(39) (a) Hotop, H.; Lineberger, W. C. *J. Phys. Chem. Ref. Data* **1975**, *4*, 539. (b) Lias S. G.; Bartmess, J. E.; Liebman, J. F.; Holmes, J. L.; Levin, R. D.; Mallard, W. G. *J. Phys. Chem. Ref. Data* **1988**, *17* (Suppl. 1). (c) Lide, D. R., Ed. *CRC Handbook of Chemistry and Physics*, *Ref. Data*, 75th ed.; CRC Press: Boca Raton, 1995; pp 9−51.

(40) Glauser, W. A.; Koszykowski, M. L. *J. Phys. Chem.* **1991**, *95*, 10705.

(41) Bradforth, S. E.; Arnold, D. W.; Metz, R. B.; Weaver, A.; Neumark, D. M. *J. Phys. Chem.* **1991**, *95*, 8066.

(42) Bendale, R.; Yang, Y. Private communication.

(43) Del Bene, J. E. *J. Phys. Chem.* **1988**, *92*, 2874.